Refereed Proceedings

The 12th International Conference on Fluidization - New Horizons in Fluidization Engineering

Engineering Conferences International *Year* 2007

Effect of Particle Size Distribution on the Performance of a Catalytic Fluidized Bed Reactor

Sanjib das Sharma* Todd S. Pugsley†

*University of Saskatchewan

†University of Saskatchewan, todd.pugsley@usask.ca

das Sharma and Pugsley: Effect of PSD on the Performance of a Fluid Bed Reactor

EFFECT OF PARTICLE SIZE DISTRIBUTION ON THE PERFORMANCE OF A CATALYTIC FLUIDIZED BED REACTOR

Sanjib das Sharma and Todd Pugsley
Department of Chemical Engineering
The University of Saskatchewan
57 Campus Drive
Saskatoon SK Canada
T: 1-306-966-4761; F: 1-306-966-4777; E: todd.pugsley@usask.ca

ABSTRACT

Computational Fluid Dynamics (CFD) has been used to model ozone decomposition in a two-dimensional fluidized bed of 2.0 meters height and 0.1 m width. Simulations were carried out with mono-size, bimodal, and wide catalyst particle size distributions with the same mean diameter to model the effect of fines on the reaction. CFD predictions fall within 20% of the experimental data.

INTRODUCTION

Fluidized bed technology facilitates the effective use of fine, highly active catalysts. However, improper design and/or operation of fluidized bed reactors can lead to conversions that fall well below the theoretical lower limit of perfectly mixed flow. It has been shown [1] that this is due to bypassing of reactant gas trapped inside bubbles, resulting in poor gas-solid contacting.

Previous experimental works [e.g. 2, 3, 4, 5] have established that the addition of fines can increase conversion in fluidized bed reactors. Sun and Grace [2] and Grace and Sun [3] have reported that, apart from the improvement in the reactor performance in a fluidized bed with a broad particle size distribution, catalytically active fines are more effective in boosting conversion than catalytically active coarse particles.

The heterogeneous ozone decomposition reaction has been used by researchers for many years to quantify gas-solids contacting in fluidized bed catalytic reactors [e.g. 2, 3, 6, 7]. This method is attractive because the reaction requires only low concentrations of the reactant, detection is rapid and accurate, and there is a measurable reaction rate at ambient conditions. Furthermore, owing to the low reactant concentrations, density and temperature changes due to reaction can be neglected and, since reactants are pre-mixed, the influence of gas-solid contacting within the reactor is isolated.

The 12th International Conference on Fluidization - New Horizons in Fluidization Engineering, Art. 80 [2007]

While ozone decomposition in a fluidized bed reactor has been extensively studied in several experimental works, the only previous computational fluid dynamics (CFD) modeling effort is that of Syamlal and O'Brien [8]. The catalyst in their model was a Geldart B powder and, while agreement was good between their model and experimental data, they used a single mean particle diameter rather than the particle size distribution in the model. In the present work, we use CFD to model the catalytic decomposition of ozone in a fluidized bed reactor containing a Geldart A catalyst powder. The main objective of the study is to model the influence of particle size distribution on the reaction. The model will be validated by comparison with the experimental data of Sun and Grace [2] and Grace and Sun [3].

COMPUTATIONAL FLUID DYNAMICS (CFD) MODEL

In the present work, we use the Eulerian CFD modeling approach in which the gas and solid phases are treated as fully interpenetrating continua. This involves the solution of the fundamental equations of mass and momentum conservation subject to suitable constitutive equations that describe the rheological properties of each phase and the interactions between the phases.

The governing equations are summarized in Table 1 for the general case of 'M' solid phases. For M = 1, the model reverts to the mono-size particle case (i.e. a single solid phase with size corresponding to the mean diameter). For a two-dimensional model such as the one developed in the present study, there are 2M+2 dependent variables to be solved: voidage, gas pressure, and 2M velocity components (2 per phase). This is done by numerically solving the coupled non-linear set of partial differential equations, as will be described later.

Constitutive relations for the gas-phase stress ($\overline{\overline{\tau}}_g$) granular stress ($\overline{\overline{S_{sm}}}$) gas-solids drag (F_{gm}) and solids-solids drag (F_{sml}) are summarized in Table 2. The only interaction forces considered between the gas and solid phases are drag and buoyancy; the particle-particle collision and frictional forces are grouped into the granular stress term.

The constants K_{1m} to K_{4m} in Equations (18) to (21) are defined as follows:

$$K_{1m} = 2(1+e_{mm})\rho_{sm} g_{0mm} \tag{25}$$

$$K_{2m} = \frac{4 d_{pm}\rho_{sm}(1+e_{mm})\varepsilon_{sm} g_{0mm}}{3\sqrt{\pi}} - \frac{2}{3}K_{3m} \tag{26}$$

$$K_{3m} = \frac{d_{pm}\rho_{sm}}{2}\left\{\frac{\sqrt{\pi}}{3(3-e_{mm})}\left[1+0.4(1+e_{mm})(3e_{mm}-1)\varepsilon_{sm} g_{0mm}\right] + \frac{8\varepsilon_{sm} g_{0mm}\left(1+e_{mm}\right)}{5\sqrt{\pi}}\right\} \tag{27}$$

$$K_{4m} = \frac{12\left(1-e_{mm}^2\right)\rho_{sm} g_{0mm}}{d_{pm}} \tag{28}$$

The granular energy equation (Equation (24)) may be solved to obtain the following expression for the granular temperature:

$$\Theta_m = \left\{ \frac{-K_{1m}\varepsilon_{sm} tr\left(\overline{\overline{D_{sm}}}\right) + \sqrt{K_{1m}^2 tr^2\left(\overline{\overline{D_{sm}}}\right)\varepsilon_{sm}^2 + 4K_{4m}\varepsilon_{sm}\left[K_{2m} tr^2\left(\overline{\overline{D_{sm}}}\right) + 2K_{3m} tr\left(\overline{\overline{D_{sm}^2}}\right)\right]}}{2\varepsilon_{sm}K_{4m}} \right\}^2 \tag{29}$$

Table 1 – Governing equations for the gas and solid phases.

Description	Equation
Volume fraction	$\varepsilon_g + \sum_{m=1}^{M} \varepsilon_{sm} = 1$ (1)
Gas phase continuity	$\frac{\partial}{\partial t}\left(\varepsilon_g \rho_g\right) + \nabla.\left(\varepsilon_g \rho_g \vec{v}_g\right) = \sum_{n=1}^{N_g} R_{gn}$ (2)
Solid phase continuity	$\frac{\partial}{\partial t}\left(\varepsilon_{sm} \rho_{sm}\right) + \nabla \cdot \left(\varepsilon_{sm} \rho_{sm} \vec{v}_{sm}\right) = \sum_{n=1}^{N_s} R_{sn}$ (3)
Species balance	$\frac{\partial}{\partial t}\left(\varepsilon_g \rho_g X_{gn}\right) + \nabla.\left(\varepsilon_g \rho_g X_{gn} \vec{v}_g\right) = R_{gn}$ (4)
Gas-phase momentum	$\frac{\partial}{\partial t}\left(\varepsilon_g \rho_g \vec{v}_g\right) + \nabla \cdot \left(\varepsilon_g \rho_g \vec{v}_g \vec{v}_g\right) = -\varepsilon_g \nabla P_g + \nabla \cdot \overline{\overline{\tau}} + \sum_{m=1}^{M} F_{gm}\left(\vec{v}_{sm} - \vec{v}_g\right) + \varepsilon_g \rho_g \vec{g}$ (5)
Solid phase momentum	$\frac{\partial}{\partial t}\left(\varepsilon_{sm} \rho_{sm} \vec{v}_{sm}\right) + \nabla \cdot \left(\varepsilon_{sm} \rho_{sm} \vec{v}_{sm} \vec{v}_{sm}\right) = -\varepsilon_{sm} \nabla P_g + \nabla \cdot \overline{\overline{S_{sm}}} - F_{gm}\left(\vec{v}_{sm} - \vec{v}_g\right) + \varepsilon_{sm} \rho_{sm} \vec{g} + \sum_{l=1}^{M} F_{sml}\left(\vec{v}_{sm} - \vec{v}_{sl}\right)$ (6)

The key assumptions in the model are as follows:

- The fractional scale factors C and C_2 are introduced into the drag function equations as per McKeen and Pugsley [9]. The value of C_2 is adjusted to ensure no segregation of the catalyst in the bed. The value of C is 0.25 [9].
- Gas-phase turbulence is dampened by the presence of the particles [10].
- The critical packing (ε_g*) and the close-packed voidage (ε^{cp}) are equal to the minimum fluidization voidage.

GEOMETRY, BOUNDARY CONDITIONS, AND NUMERICAL SOLUTION

The two-dimensional model geometry defined in the present study is based on the experimental test bed of Sun and Grace [2] and Grace and Sun [3], which was 2 m in height and 0.1 m inside diameter. The bed mass modeled in the present study was 2.75 kg, corresponding to a static bed height of 0.43 m.

The 12th International Conference on Fluidization - New Horizons in Fluidization Engineering, Art. 80 [2007]

Table 2 – Constitutive equations for the gas and solids phases

Description	Equation
Gas-solid drag	$F_{gm} = C\left(\frac{17.3}{\mathrm{Re}_m} + 0.336\right)\frac{\rho_g \left\vec{v}_{sm} - \vec{v}_g\right\vert}{d_{pm}} \varepsilon_{sm}\varepsilon_g^{-1.8}$ (7)
Solid-solid drag	$F_{sml} = C_2 \frac{3(1+e_{lm})(\pi/2 + C_{flm}\,\pi^2/8)\varepsilon_{sl}\rho_{sl}\varepsilon_{sm}\rho_{sm}(d_{pl}+d_{pm})^2 g_{0lm}\left\vec{v}_{sl} - \vec{v}_{sm}\right\vert}{2\pi\left(\rho_{sl}d_{pl}^3 + \rho_{sm}d_{pm}^3\right)}$ (8)
Gas stress	$\overline{\overline{\tau_g}} = 2\mu_g \overline{\overline{D_g}} - \frac{2}{3}\mu_g tr\left(\overline{\overline{D_g}}\right)\overline{\overline{I}}$ (9)
Granular stress	$\overline{\overline{S_{sm}}} = -P_{sm}^p \overline{\overline{I}} + \overline{\overline{\tau_{\mathrm{sm}}^{\mathrm{p}}}}$ if $\varepsilon_{\mathrm{g}} \le \varepsilon_g^*$ (10) $\overline{\overline{S_{sm}}} = -P_{sm}^v \overline{\overline{I}} + \overline{\overline{\tau_{\mathrm{sm}}^{\mathrm{v}}}}$ if $\varepsilon_{\mathrm{g}} \rangle \varepsilon_g^*$ (11)
Solids pressure (plastic regime)	$P_{sm}^p = \varepsilon_{sm} P_{sm}^*$ (12) $P_{sm}^* = 10^{25}\left(\varepsilon_{sm} - \varepsilon_{sm}^{cp}\right)^{10}$ (13)
Stress tensor (plastic regime)	$\overline{\overline{\tau}}_{sm}^{p} = 2\mu_{sm}^p \overline{\overline{D_{sm}}}$ (14) $\mu_{sm}^p = P_{sm}^p \sin\phi / 2\sqrt{I_{2Dsm}}$ (15)
2nd invariant of the strain rate tensor	$I_{2Dsm} = \frac{1}{6}\left[\left(D_{sm11} - D_{sm22}\right)^2 + \left(D_{sm22} - D_{sm33}\right)^2 + \left(D_{sm33} - D_{sm11}\right)^2\right] + D_{sm12}^2 + D_{sm23}^2 + D_{sm31}^2$ (16)
Rate of strain tensor	$\overline{\overline{D_{sm}}} = \frac{1}{2}\left[\nabla\vec{v}_{sm} + \left(\nabla\vec{v}_{sm}\right)^T\right]$ (17)
Solids pressure (viscous regime)	$P_{sm}^v = K_{1m}\varepsilon_{sm}^2\Theta$ (18)
Stress tensor (viscous regime)	$\overline{\overline{\tau_{sm}^v}} = \lambda_{sm}^v tr\left(\overline{\overline{D_{sm}^v}}\right)\overline{\overline{I}} + 2\mu_{sm}^v \overline{\overline{D_{sm}}}$ (19) $\mu_{sm}^v = K_{3m}\varepsilon_{sm}\sqrt{\Theta_m}$ (20)
2nd coefficient of viscosity	$\lambda_{sm}^v = K_{2m}\varepsilon_{sm}\sqrt{\Theta_m}$ (21)
Radial dist. functions	$g_o = \frac{1}{\varepsilon_g} + \frac{3\varepsilon_s}{2\varepsilon_g^2}$ [mono-size] (22) $g_{0lm} = \frac{1}{\varepsilon_g} + \frac{3d_{pl}d_{pm}}{\varepsilon_g^2(d_{pl}+d_{pm})}\sum_{m=1}^{M}\frac{\varepsilon_{sm}}{d_{pm}}$ [hard sphere mix] (23)
Granular energy	$(-P_{sm}^*\overline{\overline{I}} + \overline{\overline{\tau_{sm}}})\nabla\vec{v}_{sm} - \gamma_{sm} = 0$ (24)

In the experimental studies [2, 3], three catalyst mixtures of different size distributions (denoted as monosize, bimodal, and wide), but the same mean

diameter (60 μm) were examined for their influence on reactor performance. In the present modeling study, the catalyst mixtures are represented numerically by one or more solid 'species'. For the monosize case, there is one solid species with a 60 μm diameter. The bimodal mixture consists of 40 and 80 μm species with respective mass fractions of 0.47 and 0.53. For the wide size distribution, nine species with the same mass fractions as those given in the original experimental studies are defined in the model.

The inlet boundary condition was defined as uniform distribution of the fluidizing gas at a temperature of 27°C; the outlet boundary condition was a specified constant pressure (atmospheric). At the walls, the no slip condition was applied for the gas-phase while the partial slip condition was used for the solids. These conditions are consistent with our earlier modeling work [11]. The bed was assumed to be at minimum fluidization voidage conditions initially. The solid velocity was initially set to zero, while the gas velocity inside the bed was set to the interstitial gas velocity at minimum fluidization conditions. From the upper bed surface to the exit of the test vessel, the gas velocity was set equal to the minimum fluidization velocity.

The governing partial differential equations were discretized and solved numerically using the CFD code MFIX (www.mfix.org) developed in the National Energy Technology Laboratory (NETL) of the United States Department of Energy. There are many different schemes available within MFIX for discretizing the governing partial differential equations. The second order Superbee is used in the present study as it has been reported to give better resolution of bubbles [12]. All numerical solution parameters (i.e., under-relaxation, sweep direction, linear equation solvers, and residual tolerances) were left as their default values in MFIX. Adaptive time stepping was used in all the simulations, which alters the time step depending upon the stability and convergence of the solution. The MFIX simulations were run using a distributed-memory parallel version of MFIX on the Bioinformatics and Computational Biology Research Laboratory (BIRL) Beowulf computer cluster at the University of Saskatchewan.

From the initial conditions, fluidizing air was introduced uniformly into the bottom of the bed, which initiated a transient period of bed expansion and increasing voidage. For all the superficial gas velocities used in this study, the initial transient period lasted for 5 s of real time. An additional 15 s of real time was modeled after the initial transient. The 20 s of real-time fluidization modeling required 1 week of computation time for the monosize particles and about 2 weeks for the bimodal particles. However, with a wide particle distribution (nine different solid species), the simulation time was 3 months for 20 seconds of real-time.

RESULTS AND DISCUSSION

The time-averaged ozone conversion was obtained by averaging the outlet concentration of ozone between 7 seconds and 20 seconds. The CFD model predictions so obtained were compared with the experimental test data of Sun and Grace [2] for a catalyst mass of 2.75 kg and the three different catalyst size

The 12th International Conference on Fluidization - New Horizons in Fluidization Engineering, Art. 80 [2007]

distributions. The results are presented in terms ozone conversion as a function of the dimensionless reaction rate constant k'_f:

$$k'_f = \frac{k_r H_{mf}\left(1-\varepsilon_{mf}\right)}{U} \tag{30}$$

where k_r is the first-order reaction rate constant.

Figure 1 present the CFD predictions of ozone conversion for the three different particle size distributions. The model predicts the expected trend of increasing conversion with the higher values of the rate constant. The model also predicts the trends observed by Sun and Grace [2] that, for a given value of the rate constant, the catalyst consisting of a wide size distribution gives the highest conversion, followed by the bimodal and then the narrow PSD.

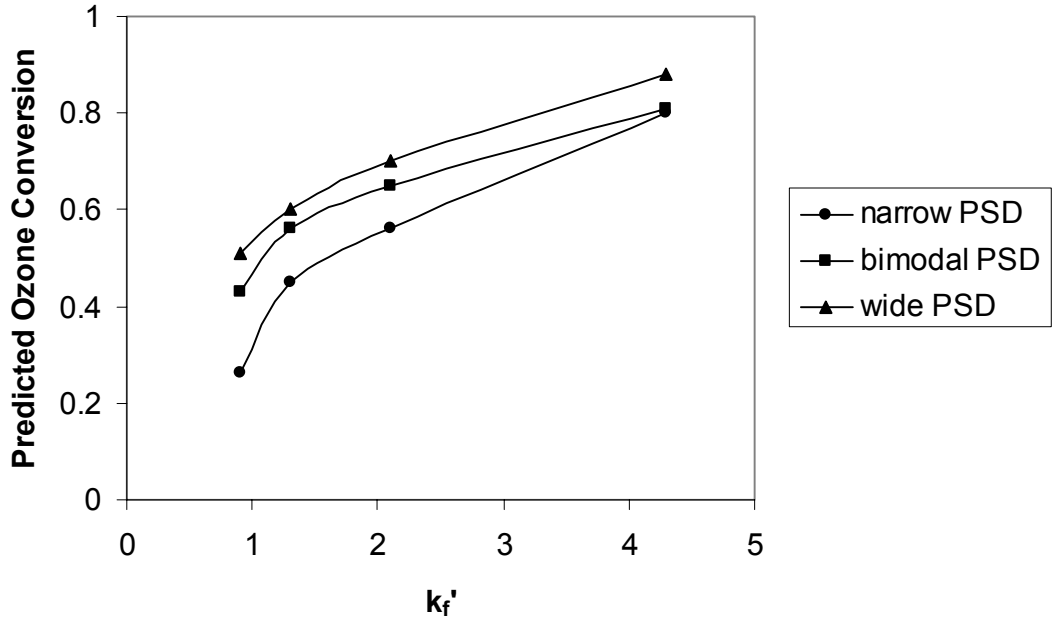

Figure 1 – CFD predictions of ozone conversion as a function of dimensionless rate constant for the three different size distributions.

Figure 2 presents a quantitative comparison of model predictions and experimental data. It can be seen that the model systematically predicts higher conversion values than the experimental data. Still, agreement is very good, with the model predictions being within 20% of the data in all cases.

To demarcate the effect of the fines from that of the coarse particles, separate simulations were carried out for the bimodal distribution with only the fines as catalytically active and with only coarse particles as active. The results are presented in Figure 3 where it can be seen that, when only the fines are active, conversion is much lower. However, when the coarse particles are made active, the conversion achieved is only slightly lower than that obtained when all the particles

are active. This trend could simply be due to the lower mass fraction of the catalyst being active, however it is contrary to the results reported by Sun and Grace [2] who explained their observations of increased conversion with the fines active as being due to increased concentration of finer catalyst particles inside the bubbles. Such a difference between the experimental observation and CFD predictions could be attributed to the fact that, although reported bimodal, the actual particle size distribution had a significant amount fines (less than 20 microns). In the CFD simulations, the fine particles were 40 microns. The presence of fines less than 20 microns increases the fine particle concentration within the bubbles containing the reacting ozone. The rest of the bed which contains the inactive coarser particles does not have much effect. For the same reason when the fine particles are made inactive, the conversion falls dramatically.

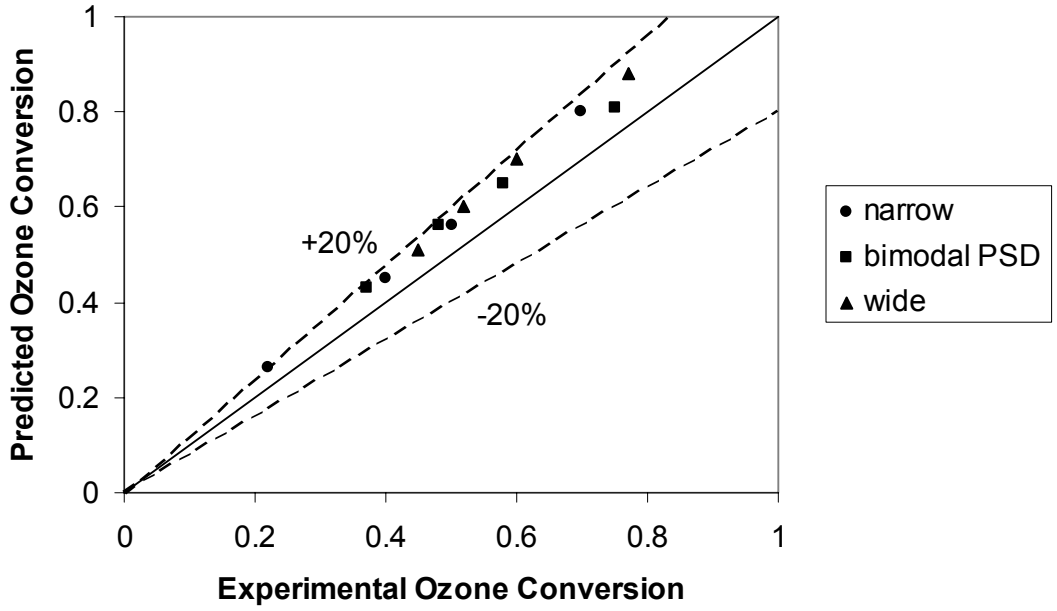

Figure 2 – Parity plot comparing the model predictions with experimental ozone conversion data of Sun and Grace [2].

CONCLUSION

Reaction kinetics for the decomposition of ozone were incorporated into a CFD model of a bubbling fluidized bed. The model predictions of ozone conversion agree to within 20% of the experimental data of Sun and Grace [2]. When only the fines fraction in the bimodal catalyst size distribution is made active, the trend in ozone conversion predicted by the model is opposite to that reported experimentally. This is likely due to the absence of fines inside the bubble in the CFD model predictions.

NOMENCLATURE

Due to space constraints, the reader is referred to our recent paper in the AIChE Journal [11] for a complete list of symbols and their definitions.

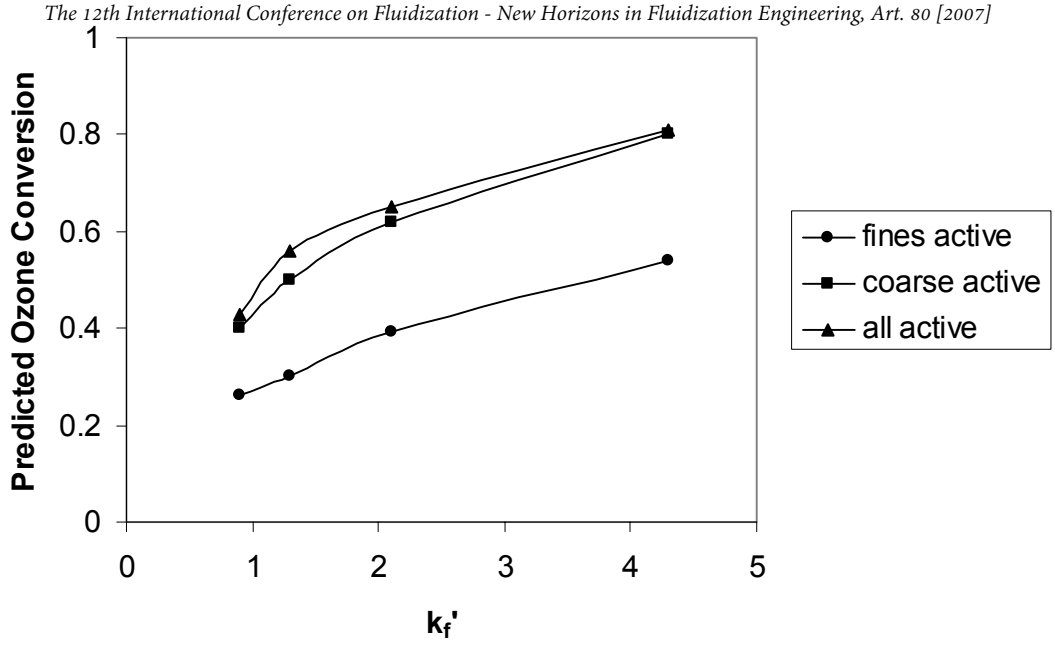

Figure 3 – CFD predictions of ozone conversion as a function of dimensionless rate constant showing the influence of active fines on conversion.

REFERENCES

1. Levenspiel, O., "Chemical Reaction Engineering", 3rd Ed., Wiley, New York, NY (1999), pp. 447 - 463.
2. Sun, G. and Grace, J.R., The effect of particle size distribution on the performance of a catalytic fluidized bed reactor, *Chem. Eng. Sci.*, 45, 2187 – 2194 (1990).
3. Grace, J. R. and Sun, G., Influence of particle size distribution on the performance of fluidized bed reactors, *Can. J. Chem. Eng.*, 69, 1126 - 1134 (1991).
4. Yates, J. G. and Newton, D., Fine particle effects in a fluidized-bed reactor, *Chem. Eng. Sci.,* 41, 801 - 806 (1986).
5. Zenz, F. A and Othmer, D.F., "Fluidization and Fluid-Particle Systems", Reinhold Publishing Corp., New York, NY (1960), pp 116 - 127.
6. Fryer, C. and Potter, O. E., Experimental investigation of models for fluidized bed catalytic reactors, *AIChE J.*, 22, 38 (1976).
7. Ouyang, S. J., Lin, J., and Potter, O. E, Ozone decomposition in a 0.254 m diameter circulating fluidized bed reactor, *Powder Technol.*, 74, 73 (1993).
8. Syamlal, M. and O'Brien, T. J., Fluid dynamic simulation of O_3 decomposition in a bubbling fluidized bed, *AIChE J.*, 49, 2793 – 2801 (2003).
9. McKeen, T. R. and Pugsley, T., Simulation and experimental validation of a freely bubbling bed of FCC catalyst, *Powder Technol.*, 129, 139 – 152 (2003).
10. Enwald, H., Peirano, E., and Almstedt, A. E., Eulerian two-phase flow theory applied to fluidization, *Int. J. Multiph. Flow*, 22 (suppl.), 21 - 66 (1996).
11. Das Sharma, S., Pugsley, T., and Delatour, R., Three-dimensional CFD model of the deaeration rate of FCC particles, *AIChE J.* 52, 2391 – 2400 (2006).
12. Guenther, C. and Syamlal, M. The effect of numerical diffusion on isolated bubbles in a gas-solid fluidized bed, *Powder Technol.,* 116, 142 - 154 (2003).